Ferroelastic shear bands in Pb3(PO4)2

Suzhi Li, Ulli Bismayer, Xiangdong Ding, and Ekhard K. H. Salje

Citation: Applied Physics Letters **108**, 022901 (2016); doi: 10.1063/1.4939853
View online: http://dx.doi.org/10.1063/1.4939853
View Table of Contents: http://scitation.aip.org/content/aip/journal/apl/108/2?ver=pdfcov
Published by the AIP Publishing

Ferroelastic shear bands in $Pb_3(PO_4)_2$

Suzhi Li,[1] Ulli Bismayer,[2] Xiangdong Ding,[1] and Ekhard K. H. Salje[3,1,a)]
[1]*State Key Laboratory for Mechanical Behavior of Materials, Xi'an Jiaotong University, Xi'an 710049, China*
[2]*Mineralogisch-Petrographisches Institut, University of Hamburg, Grindelallee 48, 20146 Hamburg, Germany*
[3]*Department of Earth Sciences, University of Cambridge, Cambridge CB2 3EQ, United Kingdom*

(Received 5 November 2015; accepted 31 December 2015; published online 11 January 2016)

We report shear bands as a precursor structure of deformation twinning in $Pb_3(PO_4)_2$. Atomic force microscopy shows "slip-line" like traces on the surface of untwinned regions of the sample. The traces are shear bands oriented along twin boundaries of the ferroelastic $R\bar{3}m$-C2/c transition. Computer simulations reproduce the shear band patterns and show that each shear band is a precursor embryo of a twin wall that forms under higher shear stress. This observation reveals the structural origin of twin boundaries under stress conditions just before ferroelastic switching occurs.
 [http://dx.doi.org/10.1063/1.4939853]

Plastic deformation in metals generates characteristic slip lines on sample surfaces where stress induces changes of the stacking of lattice planes. These slip lines have been widely investigated using atomic force microscopic (AFM) methods.[1–7] The orientation of slip lines is determined crystallographically; a typical example is the appearance of slip lines in Al where *in situ* atomic force microscopy was used to observe the structure and evolution of slip bands in plastically deformed single crystals.[7] Both the structure and the evolution of the slip bands were analyzed as functions of the tensile axis. Near the [001] tensile axis, slip bands were observed to grow to a height of approximately 250 nm with 2% plastic strain. Other slip bands were found near the stable [112] orientation, and wavy slip bands in which multiple systems are active were observed near the [111] tensile axis. In complex ceramics and crystal structures with large unit cells, such slip bands are usually prohibited by their large interfacial energy. Nevertheless, here we report AFM observations of surface pattern of the archetypal ferroelastic material $Pb_3(PO_4)_2$, which is indistinguishable from slip lines in metals. We will show that the physical origin of these line patterns is not the restacking of atomic planes, however. Instead they are shear-bands, which appear as an embryonic feature before the sample decays into a multitude of twin domains. It is the purpose of this paper to show the structural origin of these shear-bands by computer simulation in a simple ferroelastic model.

The discovery of ferroelastic shear bands has significance beyond the fact that it clarifies the appearance of hitherto unknown ferroelastic pattern under weak stress. During ferroelastic phase transitions, the elastic softening is described by the mobility of twin walls. This softening can now be attributed, at least in part, to the new discovered shear bands with an extremely high mobility. This, in turn, will increase the piezoelectric response in materials with ferroelastic and piezoelectric properties. Such shear bands can also lead to enhanced dielectric anomalies and significant frequency anomalies for piezoelectric logic devices.[8]

$Pb_3(PO_4)_2$ was widely investigated as the first material in which a full ferroelastic hysteresis was observed.[9] Its optical, structural, and thermodynamic properties were reported in Refs. 10–13. AFM images were obtained by using tapping atomic force acoustic microscopy applied to a non-etched, cleaved crystal surface. A commercial atomic force microscope (Dimension 3000, Digital Instruments) and experimental settings described in Ref. 14 were used. Figure 1 shows the three dimensional representation of the profile of ferroelastic twin structures in $Pb_3(PO_4)_2$. The height scale in Fig. 1 is 2 μm with resolution of 0.2 nm and the scan size was $8 \times 8\ \mu m^2$. The large ridges represent the primary twin boundaries formed in $Pb_3(PO_4)_2$. The fine stripes perpendicular to the primary twin boundaries are the traces of shear-bands. Their morphology is very similar to that of slip-lines but the orientation is parallel to W-type twin boundaries.[11] Figure 2

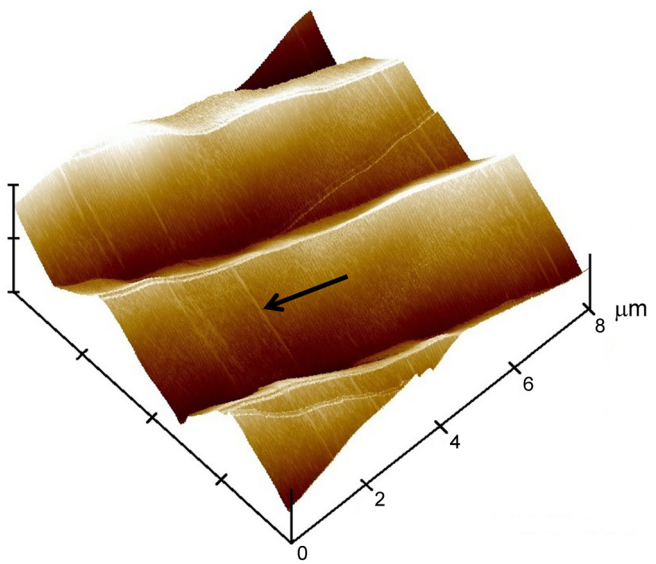

FIG. 1. Three dimensional representation of the profile of ferroelastic twin structures in $Pb_3(PO_4)_2$. The twin boundaries are the ridges in this image, while weak lines perpendicular to the twin boundaries show the "slip lines"-like shear bands, which do not lead to twinning but show significant transverse AFM contrast.

a)E-mail: ekhard@esc.cam.ac.uk

shows the AFM details of the shear bands. We can see clearly that the intersection of the shear bands and the crystal surface produce lines that are parallel to each other. The lines correspond to sites where twin boundaries typically form in other samples. It gives us the first indication that such parallel lines are a precursor of twin boundaries.

Next, we perform atomistic simulations to investigate the origin of the line patterns on an atomic scale. The formation of ferroelastic domain patterns was simulated using the standard ferroelastic model.[15] The model is constructed to be generic for all ferroelastic materials by choosing a typical spontaneous strain that leads to ferroelastic twinning. The large-scale MD simulations are performed based on the interatomic potentials, by which the elementary steps leading to the needle domain movement and kink propagation are well reproduced. Force-field simulations are not adopted, since many atomic details would be averaged and cannot be analyzed in sufficient detail. The potential consists of four interactions in a monoatomic lattice, which are (1) harmonic nearest-neighbor interactions (elastic springs), $U(r) = 20(r-1)^2$; (2) double well potentials between the next-nearest-neighbors, $U(r) = -10(r-\sqrt{2})^2 + 8000(r-\sqrt{2})^4$; (3) fourth-order interactions (elastic springs) between the third-nearest-neighbors, $U(r) = 8(r-2)^4$; and (4) a double well potential between fourth-nearest-neighbors, $U(r) = -10(r-\sqrt{5})^2 + 5100(r-\sqrt{5})^4$, where r is the interatomic distance vector. The double well potentials between the next-nearest-neighbors were designed using an inspiration from the Landau potentials to form a 2° shear angle for twinning. These interactions lead to a monoclinic structure that allows strain-compatible twinning. We use this potential to simulate the shear instability in two and three dimensions with more than 1×10^6 particles. Compared with our previous works,[15,16] we increased the nominal particle mass from 1 to 1000 to rescale the simulation temperature to reproduce the phase transition temperature, T_c. The current simulations were performed at an extremely low temperature of 0.1 K to avoid possible thermal effects on characterizing twin structure. The temperature was held constant by the Nosé–Hoover thermostat.[17,18] All simulations were carried out by using LAMMPS computer code.[19]

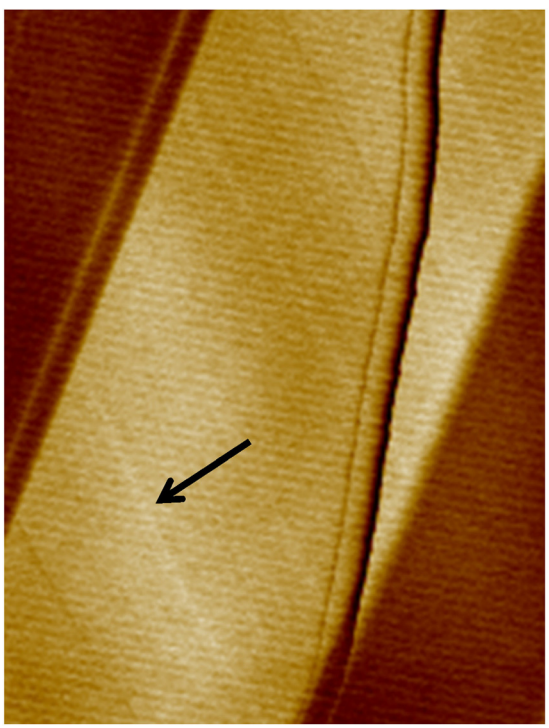

FIG. 2. Enhanced region (total width of 0.5 μm) showing twin boundaries between light and dark stripes, surface layers (vertical line), and weak "shear bands" oriented from top left to bottom right. Some of these lines meander while the overall direction is equivalent to a ferroelastic twin boundary.

The initial configuration is a two-dimensional single domain. The sample has a size of $20 \times 20\,\text{nm}^2$. We first shear the sample horizontally to generate horizontal twin boundaries. In a second step, we sheared the sample vertically to add vertical twin boundaries. The vertical shear strain was increased in small increments to observe when the additional twinning commenced. We then reduced this strain to smaller values below this threshold to remain inside the precursor regime where shear bands occur but no macroscopic twinning.

Figure 3 shows the typical images of structure evolution in the process of vertical twin formation upon different amount of external shear strain ($\varepsilon_{\text{external}}$) vertically. Figure 3(a) presents configuration at $\varepsilon_{\text{external}} = 0.890\%$, just before any noticeable structural changes appear. The horizontal twins are produced by the first shearing along horizontal direction. There is no sign for any precursor structure of vertical twins. When $\varepsilon_{\text{external}}$ is increased to 0.906%, we can see that several fine, vertical lines nucleate from each horizontal twin boundary (Fig. 3(b)). As the external shear strain is further increased ($\varepsilon_{\text{external}} = 0.912\%$), these fine vertical lines progress (Fig. 3(c)). The atomic shear strain in these lines is still rather small (around 1%), as shown in the light yellow colour in Fig. 3(c). The shear strain in these regions is far below the value in a twinned structure with a shear strain of 3.5%. These "shear-lines" do not produce sufficiently large displacements to change atomic stackings, but behave like shear bands that are induced by small displacements. When the external shear strain is further increased at $\varepsilon_{\text{external}} = 0.950\%$, these fine lines grow into vertical twins, as shown in Fig. 3(d). The atomic shear strain around twin boundaries now strongly increases, as shown by the red colour of the strain state. To have a better view of the structural evolution of twin formation, we placed the high magnification images in the right column, as marked by the frame in the left column. For the twinned structure, we draw lines between the atomic positions to trace the lattice shearing. The domain wall is needle shaped with needle tip terminated in horizontal twin boundaries, as marked in magenta colour. The profile of the needle domain matches that of the previous simulations.[20]

The simulations demonstrate that the observed shear bands are precursor structures to twin boundaries and not slip lines as seen in metals. The atomic layers in the shear bands are slightly sheared. The shear is not sufficiently to form the two twin boundaries required to form a needle domain, however. The elastic energy for a pattern with vertical twins is very high because the intersection between vertical and horizontal twin boundaries requires much greater non-local forces than isolated twin walls without intersections.[21] The driving force for the vertical twinning cannot overcome this threshold energy. Instead we find a small local shear and some deformation in the adjacent atomic layers. The total thickness of the shear band is very small (some 4 atomic

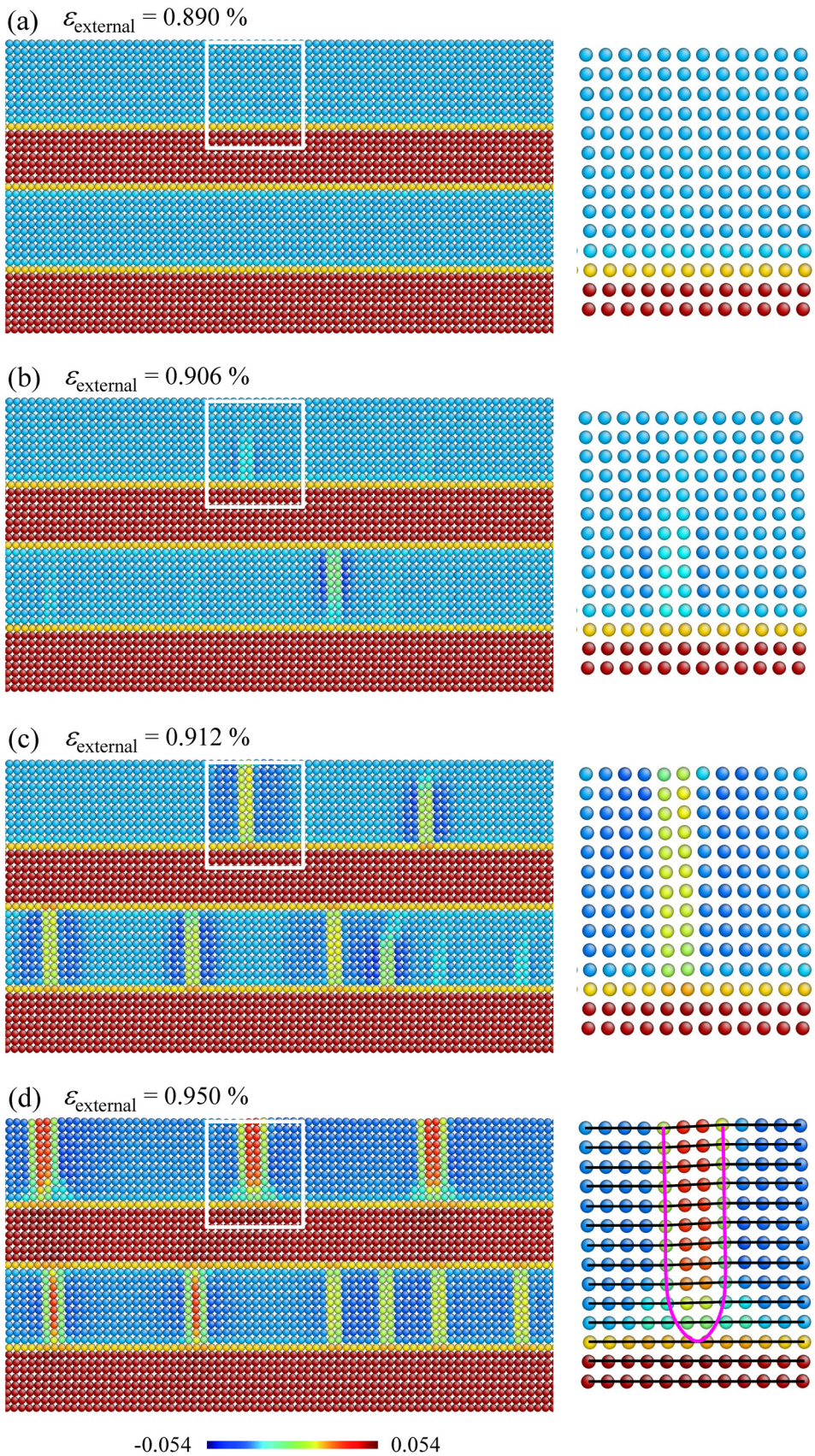

FIG. 3. Atomistic simulation of structural evolution in the process of needle twin formation upon different amount of external shear strain ($\varepsilon_{external}$). A section of the sample is cut perpendicular to the twin planes to show the nano-structure. Each atom represents a full unit cell and the colour of the atoms shows the strain amplitude at the position of each atom. The calibration bar for the local strain is shown at the bottom of the figure. (a) The structure at external strain close to the nucleation of the vertical twins, (b) nucleation of shear bands, (c) shear bands after the nucleation, and (d) formation of needle twins out of the shear bands. To have a better view of the atomic structure, high-magnification images are shown in the right column for the white frames marked in the left column. The shape of fully developed needle twin is marked in magenta with several reference lines through the atomic positions to illustrate the local lattice shear.

layers in our simulations). The faintness of the shear lines in AFM observations and their very small thickness make their experimental observation very difficult. Accordingly, their effect on the surface deformation is very small.[22] Nevertheless, we anticipate that shear lines are very common in sheared ferroelastics, in particular, when the shear stress is highly anisotropic. We can estimate their density as follows: the ratio of the distance between shear lines divided by the distance between the primary twin boundaries is around 6–10 from the experimental observation (Fig. 1) and the simulation (Fig. 3). Typical distances between the primary twin boundaries are around 10 μm for many deformed

ferroelastics. The distance between shear lines is then 1 order of magnitude smaller. This distance cannot probably be resolved in an optical microscope but is clearly within the resolution of AFM experiments. The main obstacle for their AFM observation is their faintness although we predict that strain lines as precursors for twin boundaries are very common in ferroelastics.

E.K.H.S. is grateful to EPSRC (No. EP/K009702/1) for the support. X.D. is grateful to NSFC (Nos. 51320105014, 51321003, and 51231008) for the financial support.

[1]X. J. Zheng, Y. C. Zhou, and J. Y. Li, Acta Mater. **51**, 3985 (2003).
[2]C. Tromas, J. C. Girard, V. Audurier, and J. Woirgard, J. Mater. Sci. **34**, 5337 (1999).
[3]P. Franciosi, L. T. Le, G. Monnet, C. Kahloun, and M.-H. Chavanne, Int. J. Plast. **65**, 226 (2015).
[4]Y. Liu, S. Varghese, J. Ma, M. Yoshino, H. Lu, and R. Komanduri, Int. J. Plast. **24**, 1990 (2008).
[5]T. Namazu, Y. Isono, and T. Tanaka, J. Microelectromech. Syst. **11**, 125 (2002).
[6]A. Schwab, O. Meissner, and C. Holste, Philos. Mag. Lett. **77**, 23 (1998).
[7]D. E. Kramer, M. F. Savage, and L. E. Levine, Acta Mater. **53**, 4655 (2005).
[8]P. M. Solomon, B. A. Bryce, M. A. Kuroda, R. Keech, S. Shetty, T. M. Shaw, M. Copel, L.-W. Hung, A. G. Schrott, and C. Armstrong, Nano Lett. **15**, 2391 (2015).
[9]E. K. H. Salje, Annu. Rev. Mater. Res. **42**, 265 (2012).
[10]E. K. H. Salje, A. Graeme-Barber, M. A. Carpenter, and U. Bismayer, Acta Crystallogr. B **49**, 387 (1993).
[11]U. Bismayer and E. K. H. Salje, Acta Crystallogr. A **37**, 145 (1981).
[12]U. Bismayer, J. Hensler, E. K. H. Salje, and B. Güttler, Phase Transitions **48**, 149 (1994).
[13]E. K. H. Salje and B. Wruck, Phys. Rev. B **28**, 6510 (1983).
[14]D. Bosbach, A. Putnis, U. Bismayer, and B. Güttler, J. Phys.: Condens. Matter **9**, 8397 (1997).
[15]E. K. H. Salje, X. Ding, Z. Zhao, T. Lookman, and A. Saxena, Phys. Rev. B **83**, 104109 (2011).
[16]X. Ding, T. Lookman, Z. Zhao, A. Saxena, J. Sun, and E. K. H. Salje, Phys. Rev. B **87**, 094109 (2013).
[17]S. Nosé, J. Chem. Phys. **81**, 511 (1984).
[18]W. G. Hoover, Phys. Rev. A **31**, 1695 (1985).
[19]S. Plimpton, J. Comput. Phys. **117**, 1 (1995).
[20]J. Novak, U. Bismayer, and E. K. H. Salje, J. Phys.: Condens. Matter **14**, 657 (2002).
[21]E. K. H. Salje and Y. Ishibashi, J. Phys.: Condens. Matter **8**, 8477 (1996).
[22]J. Novak and E. K. H. Salje, J. Phys.: Condens. Matter **10**, L359 (1998).